ISSN 1070-3632, Russian Journal of General Chemistry, 2018, Vol. 88, No. 2, pp. 271–276. © Pleiades Publishing, Ltd., 2018.
Original Russian Text © A.V. Pulya, I.I. Seifullina, L.S. Skorokhod, V.G. Vlasenko, A.L. Trigub, I.M. Rakipov, 2018, published in Zhurnal Obshchei Khimii, 2018, Vol. 88, No. 2, pp. 294–299.

Synthesis and Characterization of Zn(II) Complexes of 2-(7-Bromo-2-oxo-5-phenyl-2,3-dihydro-1*H*-1,4-benzodiazepin-1-yl)acetohydrazide and Its Condensation Products with Pyruvic Acid and Isatin

A. V. Pulya[a], I. I. Seifullina[a], L. S. Skorokhod[a], V. G. Vlasenko[b], A. L. Trigub[c], and I. M. Rakipov[d]

[a] *Mechnikov Odessa National University, ul. Dvoryanskaya 2, Odessa, Ukraine*
**e-mail: lborn@ukr.net*

[b] *Research Institute of Physics, Southern Federal University, Rostov-on-Don, Russia*

[c] *Kurchatov Institute National Research Center, Moscow, Russia*

[d] *Odessa National Polytechnic University, Odessa, Ukraine*

Received July 20, 2017

Abstract—The systems $ZnCl_2$–2-(7-bromo-2-oxo-5-phenyl-2,3-dihydro-1*H*-1,4-benzodiazepin-1-yl)acetohydrazide (Hydr)–propan-2-ol, $ZnCl_2$–Hydr–pyruvic acid (HPv), and $Zn(CH_3COO)_2$–Hydr–isatin(HIz)–propan-2-ol were studied. Optimal synthesis conditions were determined, and the complexes $[Zn(Hydr)_2Cl_2]$, $[Zn(HydrHPv)_2Cl_2]$, and $[Zn(HydrIz)_2]$ were isolated. The complexes were characterized by elemental analysis, thermogravimetry, IR spectroscopy, and mass spectrometry. The electrical conductivities of the complexes were measured. The local environment of the central atom in the coordination entity was determined by X-ray absorption spectroscopy.

Keywords: zinc(II) complexes, 2-(7-bromo-2-oxo-5-phenyl-2,3-dihydro-1*H*-1,4-benzodiazepin-1-yl)acetohydrazide, pyruvic acid, isatin

DOI: 10.1134/S1070363218020135

Design and research of new biologically active complexes as promising candidates for enzyme effector applications is one of the main fields of focus of the modern biocoordination chemistry. In this connection good success has been achieved with *d*-metal complexes capable of providing complete conformation compatibility of the substrate and the functional groups of the enzyme active center at all stages of the process.

We earlier studied the reactions of the vital metals Mn^{2+}, Co^{2+}, Ni^{2+}, and Cu^{2+} with 2-(7-bromo-2-oxo-5-phenyl-2,3-dihydro-1*H*-1,4-benzodiazepin-1-yl)acetohydrazide (Hydr), a known daytime tranquilizer (hydazepam), and its condensation product with pyruvic acid (HPv) [1–3]. Complexes of the latter condensation product activate *Bacillus thuringiensis var. Israelensis* IMV B-7465 peptidase about 3.5 times [4].

Proceeding with this research we reacted $ZnCl_2$ with 2-(7-bromo-2-oxo-5-phenyl-2,3-dihydro-1*H*-1,4-benzodiazepin-1-yl)acetohydrazide to obtain the complex $[Zn(Hydr)_2Cl_2]$ **1**, and the self-assembly of the systems $ZnCl_2$–Hydr–HPv and $Zn(CH_3COO)_2$–Hydr–isatin (HIz) gave the complexes $[Zn(HydrHPv)_2Cl_2]$ **2** and $[Zn(HydrIz)_2]$ **3** (Table 1). The ligand in complex **2** is a hydrazone, specifically, the condensation product of 2-(7-bromo-2-oxo-5-phenyl-2,3-dihydro-1*H*-1,4-benzodiazepin-1-yl)acetohydrazide with pyruvic acid, and the ligand in complex **3** is the condensation product of 2-(7-bromo-2-oxo-5-phenyl-2,3-dihydro-1*H*-1,4-benzodiazepin-1-yl)acetohydrazide with isatin.

Complexes **1**–**3** (Scheme 1) are finely crystalline substances insoluble in alcohols, chloroform, and acetonitrile and soluble in DMSO and DMF. The electrical conduc-tivities of 1×10^{-3} M solutions of complexes **1**–**3** in DMSO show that the complexes are nonelectrolytes (Table 1).

The thermal decomposition of complexes **1** and **2** occurs stepwise. The first, low-temperature endo effect in their TG curves is associated with a loss of two HCl

Table 1. Elemental analyses and molar electrical conductivities of complexes **1**–**3**

Comp. no.	Found, %					Formula	Calculated, %					λ, Ω^{-1} cm^2 mol^{-1}
	C	H	N	Br	Zn^{2+}		C	H	N	Br	Zn^{2+}	
1[a]	44.30	3.06	12.50	17.26	7.02	$C_{34}H_{30}Br_2Cl_2N_8O_4Zn$	44.84	3.30	12.31	17.58	7.14	11.8
2[b]	45.32	3.12	10.27	15.03	5.98	$C_{40}H_{34}Br_2Cl_2N_8O_8Zn$	45.71	3.24	10.67	15.24	6.19	10.4
3	54.43	3.00	12.28	14.32	5.81	$C_{50}H_{34}Br_2N_{10}O_6Zn$	54.79	3.11	12.79	14.61	5.94	8.1

[a] Found Cl, %: 7.62. Calculated Cl, %: 7.81. [b] Found Cl, %: 6.51. Calculated Cl, %: 6.76.

molecules. Further heating leads to melting with decomposition at 300 (**1**) and 320°C (**2**) with the subsequent burn-off of the organic part of the molecule. The TG curve of complex **3** does not display low-temperature effects, which is consistent with the results of chemical analysis (lack of solvent molecules and acetate ions). Compound **3** is stable up to 320°C, when an endo effect accompanied by a substantial weight loss takes place. Further heating causes a deep oxidative thermal decomposition of the organic part of the molecule, as evidenced by the observation of a series of high-temperature endo effects. The final thermal decomposition product of complexes **1**–**3** is ZnO, which is consistent with the weight loss in the TG curve.

The complexes proved to be difficult to volatilize under fast atom bombardment (FAB), as evidenced by low intensities of their complex and fragment ion peaks on the background of intense matrix peaks in the FAB mass spectra. The complex ions formed on

Scheme 1.

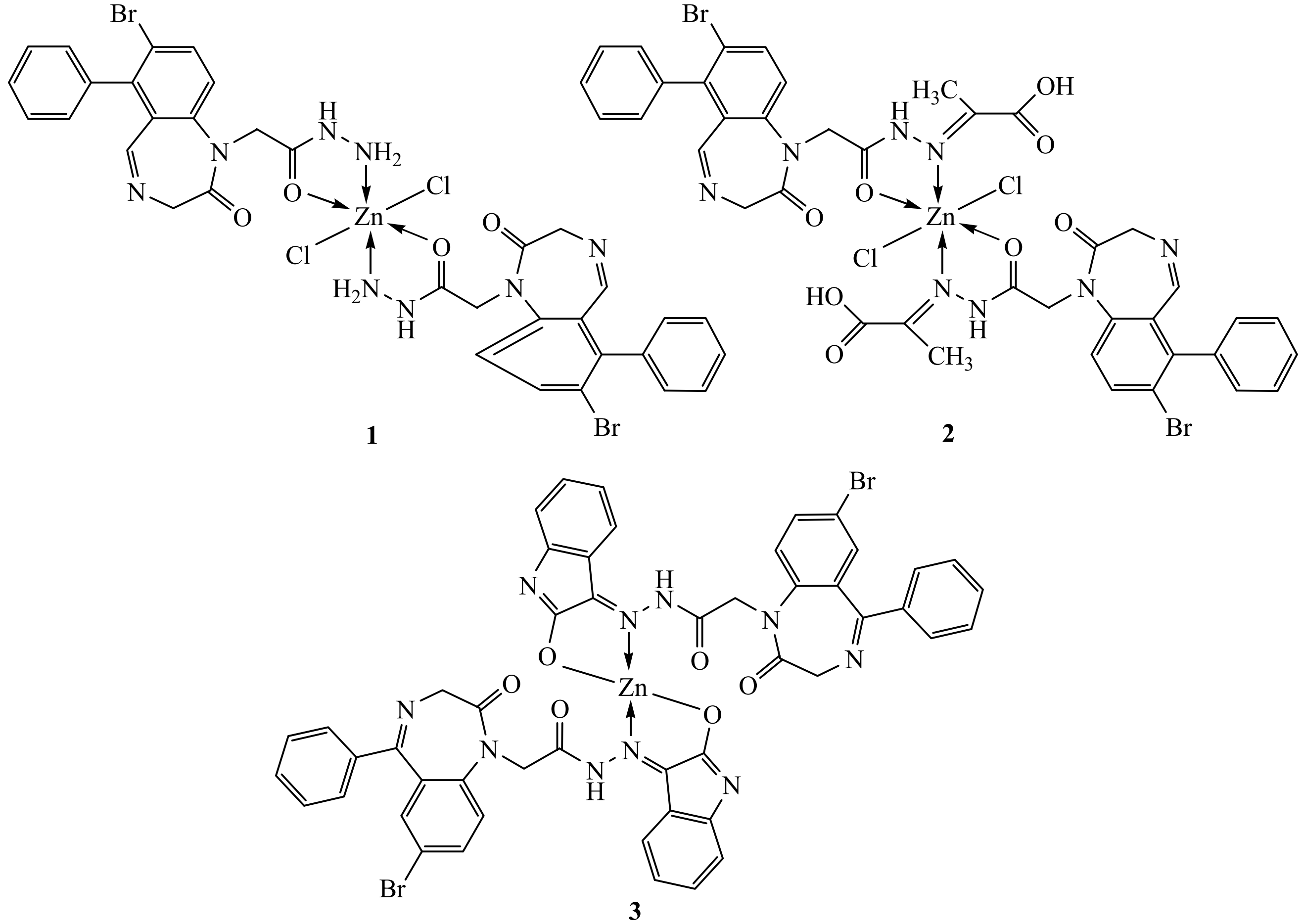

1 **2** **3**

Table 2. Mass numbers and relative peak intensities of the complex and principal fragment ions in the mass spectra of complexes **1**–**3** (intensity normalization against *m*-nitrobenzyl alcohol)[a]

Comp. no.	m/z (I_{rel}, %)						
	$[2L + Zn]^+$	$[L + Zn]^+$	$[L + ZnCl_2]^+$	$[L + H]^+$	$[L + Zn + H]^+$	$[C_{15}H_{10}BrN_2O + H]^+$	$[C_{15}H_{10}BrNO + H]^+$
1	–	–	520 (2.6)	389 (17.4)	–	315 (8.2)	301 (27.4)
2	–	520 (9.5)	–	–	–	315 (8.0)	301 (26.0)
3	1094 (5.3)	–	–	516 (16.8)	580 (19.9)	315 (10.0)	301 (44.0)

[a] L = Hydr (**1**), HydrHPv (**2**), and HydrIz (**3**).

desorption are unstable and undergo fragmentation, because they acquire excess energy after ionization. It is only the spectrum of complex **3** that shows a peak at m/z 1094, which can be assigned to the $[2L + Zn]^+$ ion, where L = HydrIz.

Analysis of the mas spectra of complexes **1**–**3** showed that the main fragmentation pathways are associated with the formation of the $[L + H]^+$ and $[L + Zn]^+$ ions, as well as the fragment ions characteriastic of the fragmentation of protonated (m/z 315 and 301). The mass numbers and intensities of the complex and fragment ions are listed in Table 2.

The mode of ligand coordination in complexes **1**–**3** was determined by IR spectroscopy by comparing the absorption bands in the spectra of the parent compounds (Hydr, HPv, and HIz) and those in the spectra of the complexes. Comparison of the spectrum complex **1** with the spectrum of the parent 2-(7-bromo-2-oxo-5-phenyl-2,3-dihydro-1*H*-1,4-benzodiazepin-1-yl)acetohydrazide reveals a low-frequency shift of the the stretching vibration bands at 3238 [ν(NH)] and 3419 cm^{-1} [ν(NH_2)] (Hydr: 3337 and 3429 cm^{-1}); change in the number and shape of the absorption bands in the ν(C=O) range: 1655 cm^{-1} (shoulder) and 1678 cm^{-1} in the spectrum of Hydr and 1664 cm^{-1} in the spectrum of complex **1**; and appearance of two new band at 511 [ν(Zn–O)] and 430 cm^{-1} [ν(Zn–N)]. These changes can be explained in terms of a bidentate binding of 2-(7-bromo-2-oxo-5-phenyl-2,3-dihydro-1*H*-1,4-benzodiazepin-1-yl)acetohydrazide to Zn^{2+}, which involves the hydrazide amino group and carbonyl oxygen.

Comparison of the IR spectra of the free ligands and their respective complexes **2** and **3** revealed a lack of the stretching vibration band of the amino group and a new ν(C=N) band at 1558 (**2**) and 1615 cm^{-1} (**3**). This finding suggests that the ligand in complexes **2** and **3** is a condensation product. In the IR spectrum of complex **2**, the hydrazide ν(C=O) band is shifted to lower frequencies [1678 (Hydr), 1669 cm^{-1} (**2**)], due to the involvement of this bond in coordination with Zn^{2+}. The IR spectrum of complex **3** displays a ν(C–O) band at 1186 cm^{-1}, which is characteristic of the deprotonated imide form of isatin coordinated to zinc(II) [5] (cf. 1202 cm^{-1} for HIz). The new bands in the spectra of complexes **2** and **3** at 511 (**2**), 553 cm^{-1} (**3**) and 459 (**2**), 450 cm^{-1} (**3**) were assigned to ν(Zn–O) and ν(Zn–N) vibrations, respectively.

Additional information on the structure of the coordination entities in complexes **1**–**3** was obtained from the X-ray absorption spectra (analysis of EXAFS and XANES). The Zn *K*-edge XANES spectra of complexes **1**–**3** are poor in information, because they scarcely contain a pre-edge structure. The first derivatives of the edges have a single base broadened peak with weakly expressed features. A deeper insight into the structure of the local environment of the coordination centers in complexes **1**–**3** was provided by an analysis of the Zn *K*-edge EXAFS spectra.

The Fourier transform modules (FTM) of the Zn *K*-edge EXAFS spectra of complexes **1** and **2** are similar to each other and contain a base peak (r = 1.80 Å) with a shoulder (r = 1.45 Å). Such patterns points to the existence of a few close coordination shells (see Figs. 1a and 1b). The FTM for complex **3** contains a base peak at r = 1.54 Å, which is associated with scattering of the photoelectron wave on the first coordination shell comprising ligand nitrogen and oxygen atoms (see Fig. 1c). The peaks at larger values in the FTMs oof complexes **1**–**3** are associated with the coordination shell comprising different ligand atoms, primarily carbons.

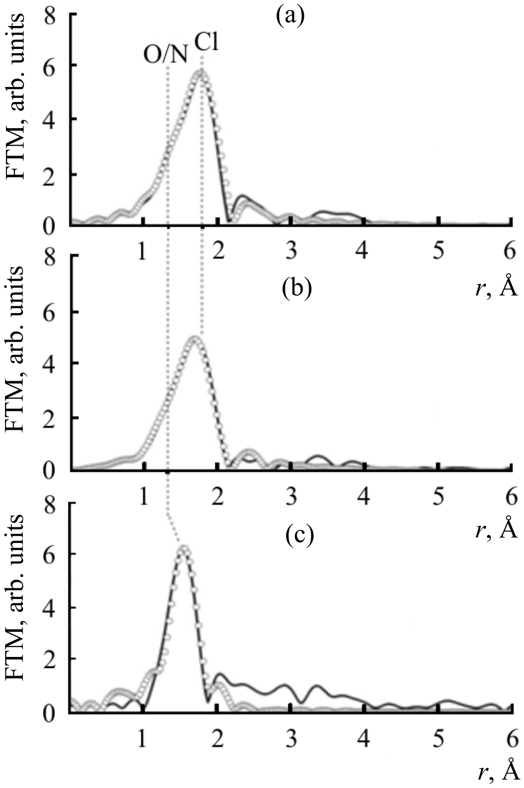

Fourier transform modules of the Zn *K*-edge EXAFS spectra of complexes (a) **1**, (b) **2**, and (c) **3**.

As follows from the calculated EXAFS spectra, the nearest coordination environment of Zn(II) in complexes **1** and **2** consists of two nitrogen and two chlorine atoms; the distances of these atoms to the central atom are listed in Table 3. Furthermore, there are coordination shells comprising two oxygen atoms at a much larger distance (2.54–2.60 Å), which complement the coordination number to 6. Such structure of the coordination entities is characteristic of zinc complexes [6, 7], we used as model compounds to calculate the scattering phases and amplitudes. The best model of the local atomic structure for complex **3** was provided by the first shell comprising four oxygen and nitrogen atoms of the tetrahedral coordination environment of the zinc atom (Table 3).

EXPERIMENTAL

Thermogravimetry was performed on a Paulik–Paulik–Erdey Q-derivatograph. Samples were heated in air from 20 to 1000°C at a rate of 10 deg/min (sample weight: 60–80 mg, sample holder: a platinum crucible without a lid, reference: calcined alumina). The molar electrical conductivity of 1×10^{-3} M solutions of complexes **1**–**3** in DMSO was measured an Ekonomiks–ekspert digital meter, the type of the electrolyte was determined using the tables in [8].

The IR spectra (4000–400 cm^{-1}) of complexes **1**–**3** pelleted with KBr were recorded on Perkin–Elmer Spectrum BX-II FI-IR and Shimadzu FTIR-8400S spectrophotometers. The MALDImass spectra were obtained on a VG 7070 instrument using fast xenon atoms of 8 keV and a *m*-nitrobenyl alcohol matrix.

The Zn *K*-edge X-ray absorption spectra of solid complexes **1**–**3** were registered in the transmission mode on an EXAFS spectrometer at the “Structural Materials Science” Center, Kurchatov Center for Synchrotron Radiation and Nanotechnologies (Moscow) [9]. The energy of the electron beam used as a source of X-ray synchrotron radiation was 2.5 GeV at a current of 80–100 мA. The X-ray radiation was monochromatized using a Si(111) double-crystal monochromator. The X-ray absorption spectra were processed by the standard procedures for background

Table 3. First-shell parameters for complexes **1**–**3**, obtained by multishell fitting of the EXAFS data[a]

Complex	N	*R*, Å	σ^2, Å^2	Coordination shell	$\Re^b$, %
1	2	2.06	0.0035	N	2.0
	2	2.27	0.0043	Cl	
	2	2.60	0.0035	O	
2	2	2.00	0.0040	N	2.2
	2	2.24	0.0040	Cl	
	2	2.54	0.0040	O	
3	2	1.98	0.0035	O/N	1.5
	2	2.03	0.0035	O/N	

[a] (*R*) Interatomic distance, (*N*) coordination number, (σ^2) Debuy–Waller factor, and ($\Re$) goodness-of-fit function.

[b] Approximation space Δr for complexes **1** and **2** and for complex **3** are 1.05–2.10 Å and 1.0–1.9 Å, respectively.

subtraction, *K*-edge normalization, and atomic absorption μ_0 isolation, after which Fourier transform of the resulting (χ) EXAFS spectra was performed in the photoelectron wave vector *k* range from 2.5 to 13 Å^{-1} with the weighting function k^3. The FTMs of the χ spectra correspond, to phase shift accuracy, to the radial atomic distribution function around an absorbing metal ion. The threshold ionization energy E_0 was taken as the maximum of the *K*-edge first derivative and then varied on fitting.

The exact first-shell parameters for the metal complexes were determined by the nonlinear least-squares fit of the corresponding structural parameters derived from the calculated EXAFS signal to those derived from the signal isolated from the full EXAFS spectrum by Fourier filtering. The nonlinear least-squares fit was performed using the IFFEFIT software package [10]. The photoelectron wave scattering phases and amplitudes necessary to construct the model spectrum were calculated using the FEFF7 software [11] with the input atomic coordinates taken from the single-crystal X-ray data for complexes with a similar atomic environment of the metal atom.

The goodness-of-fit function *Q*, which was minimized to find the first-shell parameters, was calculated by the following formula:

$$\Re = \sum_{i=1}^{N_{\text{pts}}} \frac{\{\text{Re}[\chi_{\text{data}}(R_i) - \chi_{\text{th}}(R_i)]\}^2 + \{Im[\chi_{\text{data}}(R_i) - \chi_{\text{th}}(R_i)]\}^2}{\{\text{Re}[\chi_{\text{data}}(R_i)]\}^2 + \{\text{Im}[\chi_{\text{data}}(R_i)]\}^2}.$$

Here $\chi_{\text{data}}(R_i)$ and $\chi_{\text{th}}(R_i)$ are the EXAFS functions in the *R* space and N_{pts}, number of data points in the fitted spectral region.

Elemental analysis was performed on a semiautomatic CHN analyzer; total chlorine and bromine (in complexes **1** and **2** and bromine in complex **3** were determined by mercurometry [12], and zince was determined by ICP–MS on a Perkin–Elmer Optima 2100 DV instrument.

Bis[2-(7-bromo-2-oxo-5-phenyl-2,3-dihydro-1*H*-1,4-benzodiazepin-1-yl)acetohydrazide]zinc(II) dichloride (1). A solution of $ZnCl_2$ in 10 mL of ethanol was added to a stirred solution of 2 mmol of 2-(7-bromo-2-oxo-5-phenyl-2,3-dihydro-1*H*-1,4-benzodiazepin-1-yl)acetohydrazide (Hydr) in 20 mL of propan-2-ol ($ZnCl_2$: Hydr molar ratio 1 : 2). The reaction mixture was heated under reflux on a water bath for 0.5 h. Complex **1** that precipitated after cooling was filtered off, washed with isopropanol and ethanol, and dried at 80°C to constant weight.

Bis(2-{2-[(7-bromo-2-oxo-5-phenyl-2,3-dihydro-1*H*-1,4-benzodiazepin-1-yl)acetyl]hydrazinilidene}-propanoic acid)zinc(II) dichloride (2). Pyruvic acid (HPv), 2 mmol, and a solution of $ZnCl_2$ in ethanol (10 mL) were added to a solution of 2 mmol of Hydr in 20 mL of propan-2-ol ($ZnCl_2$: Hydr : HPv molar ratio 1 : 2 : 2). The reaction mixture was heated under reflux for 1 h. Complex **2** that precipitated after cooling was treated as described for complex **1**.

Bis(3-{2-[(7-bromo-2-oxo-5-phenyl-2,3-dihydro-1*H*-1,4-benzodiazepin-1-yl)acetyl]hydrazinilidene}-indol-2-olato)zinc(II) (3). A solution of 2 mmol of isatin (HIz) in 20 mL of propan-2-ol was added to a solution of 2 mmol of Hydr in 20 mL of propan-2-ol. The reaction was heated under reflux on a water bath for 3 h and then a solution of $Zn(CH_3COO)_2{\cdot}2H_2O$ in ethanol was added ($ZnCl_2$: Hydr : HIz molar ratio 1 : 2 : 2), and refluxing was continued for an additional 1 h. Complex **3** that precipitated after cooling was washed with isopropanol and ethanol and dried at 80°C to constant weight.

ACKNOWLEDGMENTS

The work was financially supported in part by the Russian Foundation for Basic Research (project no. 16-03-00503a).

REFERENCES

1. Pulya, A.V., Seifullinna, I.I., Skorokhod, L.S., Efimov, N.N., Ugolkova, E.A., and Minin, V.V., *Russ. J. Inorg. Chem.*, 2015, vol. 60, no. 1, p. 51. doi 10.1134/S0036023615010106
2. Pulya, A.V., Seifullinna, I.I., Skorokhod, L.S., Vlasenko, V.G., Levchenkov, S.I., and Pavlovskii, V.I., *Russ. J. Gen. Chem.*, 2015, vol. 85, no. 1, p. 97. doi 10.1134/S1070363211501017X
3. Pulya, A.V., Seifullinna, I.I., Skorokhod, L.S., Efimov, N.N., Ugolkova, E.A., and Minin, V.V., *Russ. J. Inorg. Chem.*, 2016, vol. 61, no. 1, p. 38. doi 10.1134/S0036023616010204
4. Varbanets, L.D., Nidyalkova, N.A., Seifullina, I.I., Pulya, A.V., and Skorokhod, L.S., *Mikrobiol. Zh.*, 2017, vol. 79, no. 3, p. 14.

5. Nakamoto, K., *Infrared Spectra of Inorganic and Coordination Compounds*, 4th ed., New York: Wiley, 1986.
6. Muller, B. and Vahrenkamp, H., *Eur. J. Inorg. Chem.*, 1999, p. 137. doi 10.1002/(sici)1099-0682(199901) 1999:1<137::aid-ejic137> 3.0.co;2-t
7. Schneider, A. and Vahrenkamp, H., *Z. Anorg. Allg. Chem.*, 2003, vol. 629, p. 2122. doi 10.1002/zaac.200300188
8. Geary, W.J., *Coord. Chem. Rev.*, 1971, vol. 7, p. 81. doi 10.1016/S0010-8545(00)80009-0
9. Chernyshov, A.A., Veligzhanin, A.A., and Zubavichus, Ya.V., *Nucl. Instr. Meth. Phys. Res. A*, 2009, vol. 603, p. 95. doi 10.1016/j.nima.2008.12.167
10. Newville, M., *J. Synchrotron Rad.*, 2001, vol. 8, p. 96. doi 10.1107/S0909049500016290
11. Zabinski, S.I., Rehr, J.J., Ankudinov, A., and Alber, R.C., *Phys. Rev.*, 1995, vol. 52, p. 2995. doi 10.1103/PhysRevB.52.2995
12. Klyuchnikov, N.G., *Rukovodstvo po neorganicheskomu sintezu* (Manual on Inorganic Synthesis), Moscow: Khimiya, 1965, p. 104.